THE JOURNAL OF PHYSICAL CHEMISTRY A
A JOURNAL OF THE AMERICAN CHEMICAL SOCIETY

pubs.acs.org/JPCA

Article

Photoelectron Imaging and Photodetachment Spectroscopy for the Cryogenically Cooled Cyanocyclopentadienide Anion

Published as part of The Journal of Physical Chemistry A special issue "Mark A. Johnson Festschrift".

Jisoo Kang, Edward I. Brewer, Dao-Fu Yuan,* Yue-Rou Zhang, and Lai-Sheng Wang*

Cite This: *J. Phys. Chem. A* 2025, 129, 1060−1067

Read Online

ACCESS | Metrics & More | Article Recommendations | Supporting Information

ABSTRACT: The cyano-cyclopentadiene molecule (CN-C_5H_5) has attracted significant interest since its detection in the interstellar medium, but the radical (CN-C_5H_4) and anionic (CN-$C_5H_4^-$) forms of cyano-cyclopentadiene have not been studied. The cyano-cyclopentadienyl radical (CN-Cp) has a strong dipole moment, rendering it an ideal system for vibrational and rotational spectroscopy. We report an investigation of the cryogenically cooled cyano-cyclopentadienide anion (CN-Cp^-) using high-resolution photoelectron imaging, photodetachment spectroscopy, and resonant photoelectron imaging. The electron affinity of the CN-Cp radical is measured accurately to be 2.7741 ± 0.0003 eV (22,375 ± 2 cm^{-1}). A low-lying excited state is observed for the CN-Cp neutral radical at 151 cm^{-1} above the ground state. The overlap and vibronic coupling of the ground and low-lying electronic states give rise to complicated and congested photoelectron spectra. A dipole-bound state is observed for the CN-Cp^- anion with a binding energy of 94 cm^{-1}, along with 15 vibrational Feshbach resonances. Resonant photoelectron spectra via the vibrational resonances yield well-resolved spectra, allowing 26 vibronic levels to be identified for CN-Cp. The rich spectroscopic information will be valuable to compare with theoretical studies to unravel the vibronic coupling and nonadiabatic effects in the CN-Cp radical.

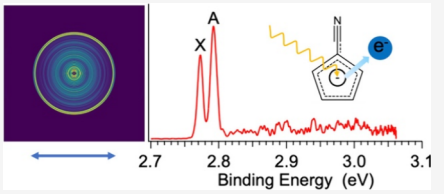

1. INTRODUCTION

Polycyclic aromatic hydrocarbons (PAHs) are contributors to the unidentified infrared emission bands in the interstellar medium (ISM), as well as the diffuse interstellar bands (DIBs).[1,2] Despite their prevalence in the ISM, the formation mechanisms of these molecules remain unclear.[3] For PAH anions, one proposed formation pathway involves dipole-bound states (DBSs) acting as doorways.[4−6] DBSs are nonvalence electronic states that anions can support if their neutral cores have sufficiently large dipole moments.[7−9] Recent studies have identified several cyano-functionalized PAHs within the Taurus Molecular Cloud (TMC-1).[10−12] The large dipole moments of these molecules, imparted by the CN group, make them ideal targets for microwave spectroscopy. In particular, the cyano-cyclopentadiene molecule (CN-C_5H_5) has attracted significant recent interest after being detected in the TMC-1.[13] The deprotonated cyano-cyclopentadienide anion (CN-$C_5H_4^-$ or CN-Cp^-) can potentially support a DBS, providing an excellent opportunity to obtain detailed spectroscopic information about the CN-Cp radical using photodetachment spectroscopy (PDS) and resonant photoelectron spectroscopy (rPES).[14] Although microwave and laser-induced fluorescence spectroscopy of the cyano-cyclopentadiene molecule and the CN-Cp radical have been reported,[15−17] very little is known about the CN-Cp^- anion or the low-lying electronic states of the CN-Cp radical. We have developed cryogenic PDS and rPES, which have yielded unprecedented vibronic information about complicated PAH species.[14,18−23] For instance, we have recently studied 2-cyanopyrrolide using both PDS and rPES, revealing 19 out of 24 fundamental vibrational modes, including 6 out-of-plane modes.[24] These methods present a promising approach to investigate the CN-Cp^- anion and the CN-Cp radical.

Herein, we report PDS, rPES, and high-resolution photoelectron images on the cryogenically cooled CN-Cp^- anion. The electron affinity (EA) of CN-Cp is accurately measured to be 2.7741 ± 0.0003 eV (22,375 ± 2 cm^{-1}). A low-lying excited electronic state is observed for the CN-Cp radical at 151 cm^{-1} above the ground state. The overlap between the two close-lying electronic states and vibronic coupling yield complex and congested photoelectron spectra, which cannot be assigned on the basis of Franck−Condon simulations. A DBS is observed for the CN-Cp^- anion with a binding energy of 94 cm^{-1}, along with 15 vibrational Feshbach resonances. Resonant photoelectron spectra via the Feshbach resonances give rise to well-resolved vibrational features, allowing 26 vibronic levels to be identified for CN-Cp. The rich spectroscopic information obtained from the PDS and rPES will be valuable to be

Received: November 10, 2024
Revised: January 9, 2025
Accepted: January 13, 2025
Published: January 17, 2025

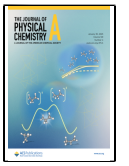

https://doi.org/10.1021/acs.jpca.4c07624
J. Phys. Chem. A 2025, 129, 1060−1067

compared with future theoretical calculations to unravel the vibronic coupling and nonadiabatic effects in the CN-Cp radical.

2. EXPERIMENTAL METHODS

2.1. Photoelectron Imaging. The experiments were performed using our third-generation ESI-PES apparatus, which has been described in detail elsewhere.[25] In brief, the apparatus is equipped with an electrospray ionization source,[26] a cryogenically cooled Paul trap,[27] and a high-resolution photoelectron imaging system.[28] The $CN\text{-}Cp^-$ anions were produced by electrospray of a 1 mM solution of cyanoferrocene (ChemScene, ≥ 97.0%) dissolved in a CH_3OH/H_2O mixed solvent (9:1 volume ratio) spiked by a few drops of NaOH. The $CN\text{-}Cp^-$ anions produced as a result of dissociation of cyanoferrocene in the ESI source were guided into the Paul trap through a series of quadrupole and octupole ion guides. The Paul trap was cryogenically cooled to 4.6 K by a close-cycle helium refrigerator. The $CN\text{-}Cp^-$ anions were trapped for roughly 0.1 s and were thermally cooled through collisions with a mixed He/H_2 (1 mTorr, 4/1 ratio in volume) background gas. The anions were extracted at a 10 Hz repetition rate into a time-of-flight mass spectrometer. The $CN\text{-}Cp^-$ anions selected by a mass gate were photodetached by a tunable dye laser, the third harmonic (3.496 eV), and the fourth harmonic (4.661 eV) of an Nd:YAG laser in the interaction zone of the VMI system. Photoelectrons were projected onto a pair of microchannel plates (75 mm in diameter) in front of a phosphor screen and the resulting photoelectron images were taken by a charge-coupled-device (CCD) camera. The raw images were analyzed using the pBasex and BASEX programs[29,30] and were calibrated using Au^- at various photon energies. The resolution of our VMI system was 3.8 cm^{-1} for the kinetic energy (KE) of 55 cm^{-1} and ∼1.5% for (ΔKE/KE) for KE higher than 1 eV.[28]

2.2. Photoelectron Angular Distributions. For randomly oriented molecules with linearly polarized light, the differential detachment cross section, $I(\theta)$, is given as[31]

$$I(\theta) = \frac{\sigma_T}{4\pi}\cdot(1 + \beta P_2(\cos(\theta))) \quad (1)$$

where σ_T represents the total detachment cross section, $P_2(\cos(\theta))$ is the second-order Legendre polynomial, and θ is the angle between the photoelectron and the polarization direction of the laser. The asymmetry parameter, β, has a range from −1 to 2. $\beta = 0$ pertains to an isotropic s outgoing wave; $\beta = 2$ indicates a p outgoing wave in which the maximum intensity occurs in the same direction as the polarization of the laser; and $\beta = -1$ indicates a $(s + d)$ outgoing wave in which the maximum intensity occurs in the direction perpendicular to the polarization of the laser.

2.3. Computational Methods. Density functional theory (DFT) was employed to calculate the electronic structure and optimize the geometries of the relevant anions and neutrals at the B3LYP/aug-cc-pVTZ level using the Gaussian 09 package.[32] Franck−Condon (FC) factors were calculated using FC-Lab2[33] and the optimized geometries of the anion and the neutral.

3. RESULTS

3.1. Nonresonant Photoelectron Imaging and Spectroscopy. We first took PE images of the $CN\text{-}Cp^-$ anion at 3.496 and 4.661 eV, as displayed in Figure 1. The spectra

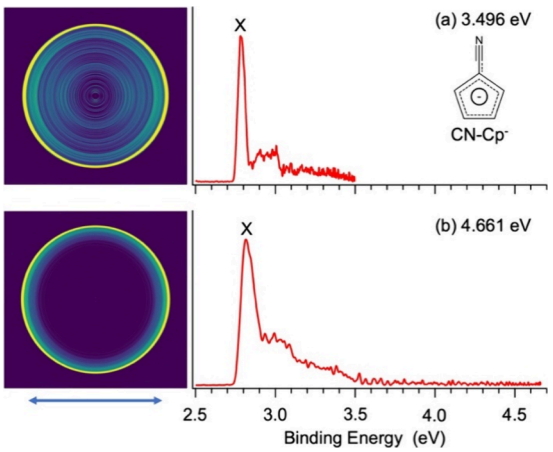

Figure 1. Photoelectron images and spectra of cryogenically cooled $CN\text{-}Cp^-$ anions at (a) 3.496 eV and (b) 4.661 eV. The double arrow below the images indicates the laser polarization direction.

represent detachment transitions from the ground state of the $CN\text{-}Cp^-$ anion to that of the neutral CN-Cp radical. Franck−Condon activities are observed up to ∼3.5 eV, but the spectra appear surprisingly complex and no vibrational fine features are resolved even at the higher spectral resolution at 3.496 eV. No other detachment transitions are observed up to 4.66 eV.

To resolve vibrational features, we took four high resolution photoelectron images at lower photon energies closer to the detachment threshold: 2.7782, 2.8583, 2.9813, and 3.0616 eV, as presented in Figure 2. The near-threshold spectrum taken at 2.7782 eV, yielded an accurate adiabatic detachment energy (ADE) of 2.7741 ± 0.0003 eV (22,375 ± 2 cm^{-1}), which is also the EA of the CN-Cp radical. An additional intense peak (A) was resolved at 2.7929 eV in the three higher photon

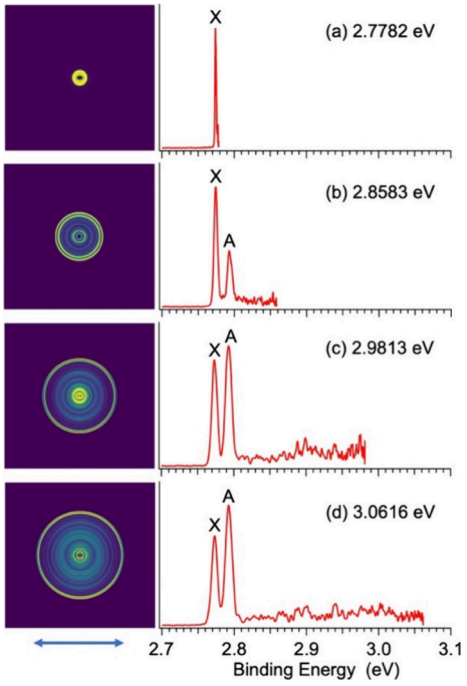

Figure 2. Photoelectron images and spectra of $CN\text{-}Cp^-$ at (a) 2.7782 eV (22,408 cm^{-1}), (b) 2.8583 eV (23,053 cm^{-1}), (c) 2.9813 eV (24,046 cm^{-1}), and (d) 3.0616 eV (24,694 cm^{-1}). The double arrow below the images indicates the laser polarization direction.

https://doi.org/10.1021/acs.jpca.4c07624
J. Phys. Chem. A 2025, 129, 1060−1067

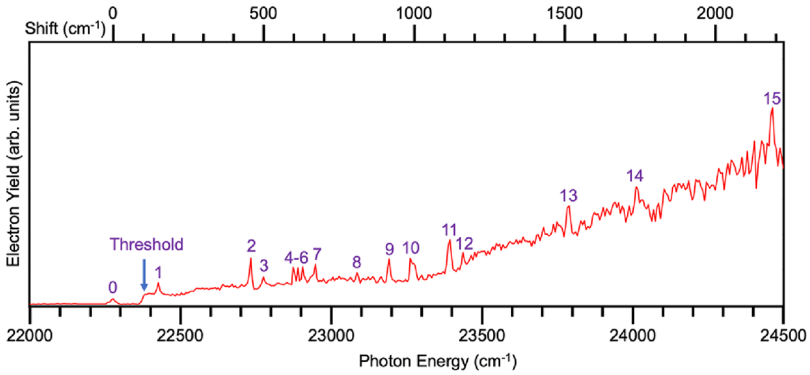

Figure 3. Photodetachment spectrum of CN-Cp$^-$. The arrow indicates the detachment threshold measured from the PES above. The top axis represents the shift relative to the vibrational ground state of the DBS marked as peak 0. The vibrational levels of the DBS are labeled as peaks 1−15.

energy spectra. It is separated from peak X by 0.01888 eV (152 cm^{-1}), but it does not appear to be a vibrational feature because its relative intensity changes with the photon energy. It is likely the origin of a low-lying electronic excited state of the CN-Cp neutral radical. Weak and congested vibrational features are observed at higher binding energies, but are not well resolved. These complicated vibronic structures are probably due to the fact that vibrational features of the two electronic states overlap or more likely due to vibronic couplings between the two states. The β values (Table S1) for the two peaks are also different, consistent with the assignments that the two peaks represent different electronic transitions.

3.2. Photodetachment Spectroscopy. The CN group in the CN-Cp radical significantly enhances its dipole moment to 3.62 D (calculated using DFT at the B3LYP/aug-cc-pVTZ level) compared to 0.420 D for the parent cyclopentadiene (Cp) molecule.[34,35] This dipole moment is higher than the 2.5 D critical value to support DBS,[7−9] suggesting that there should be a DBS below the detachment threshold of the CN-Cp$^-$ anion. To search for the DBS, we performed PDS by scanning the laser wavelength across the detachment threshold and monitoring the total electron yield, as shown in Figure 3. A distinct step is observed at 22,375 cm^{-1}, in agreement with the EA determined above from the high-resolution photoelectron (PE) spectrum (Figure 2a). The detachment cross section near the threshold exhibits *s*-wave character, according to the Wigner threshold law.[36] The weak below-threshold peak labeled as 0 at 22,278 cm^{-1} (2.7621 eV) is due to one-color resonant two-photon photodetachment (R2PD), evident of the existence of the expected DBS. This feature corresponds to the zero-point level of the DBS with a binding energy of 94 ± 5 cm^{-1} (0.0117 ± 0.0006 eV), determined by its separation from the detachment threshold. Fifteen above-threshold peaks or vibrational Feshbach resonances are observed within an energy range of approximately 2130 cm^{-1} (0.264 eV) above the threshold and are labeled from 1 to 15. These resonances stem from single-photon excitations to above-threshold vibrational levels of the DBS followed by vibrational autodetachment. The photon energies corresponding to the 15 DBS vibrational peaks and their shifts relative to peak 0 are given in Table 1.

3.3. R2PD Photoelectron Imaging. By tuning the detachment laser wavelength to peak 0, we obtained the one-color R2PD PE image and spectrum, as shown in Figure 4. There are two prominent features in the R2PD PE spectrum, denoted as "DBS" and "S_0". The DBS feature on the lower binding energy (BE) region corresponds to direct R2PD, where the first photon excites the anion to the zero-point level of the DBS, followed by detachment from the DBS by a second photon within the same laser pulse. The low BE of the DBS peak corroborates the precise measurement from the PD spectrum above (0.0117 eV or 94 cm^{-1}). The distinctive *p*-wave distribution, characterized by a β value of 1.67 ± 0.05 for the DBS image (left, Figure 4), validates the *s*-like diffuse dipole-bound orbital.

Table 1. Observed DBS Vibrational Peaks in the Photodetachment Spectrum

peak	photon Energy (eV)[a]	photon energy (cm^{-1})[a]	shift (cm^{-1})[b]
0	2.7621	22,278	0
1	2.7807	22,428	150
2	2.8187	22,735	457
3	2.8242	22,779	501
4	2.8360	22,874	596
5	2.8380	22,890	612
6	2.8399	22,906	628
7	2.8447	22,944	666
8	2.8621	23,085	807
9	2.8754	23,192	914
10	2.8843	23,264	986
11	2.9010	23,398	1120
12	2.9057	23,436	1158
13	2.9488	23,784	1506
14	2.9778	24,018	1740
15	3.0329	24,462	2184

[a]The uncertainty associated with the peak position is ±0.0006 eV or ±5 cm^{-1}. [b]The shift is relative to the BE of peak 0.

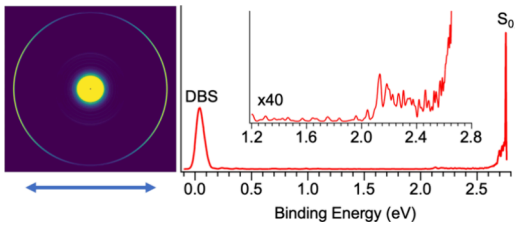

Figure 4. One-color R2PD PE image and spectrum of CN-Cp$^-$ taken at 2.7621 eV (22,278 cm^{-1}). The double arrow below the image indicates the polarization direction of the laser. The inset depicts the region from 1.2 to 2.8 eV at an ×40 scale.

https://doi.org/10.1021/acs.jpca.4c07624
J. Phys. Chem. A 2025, 129, 1060−1067

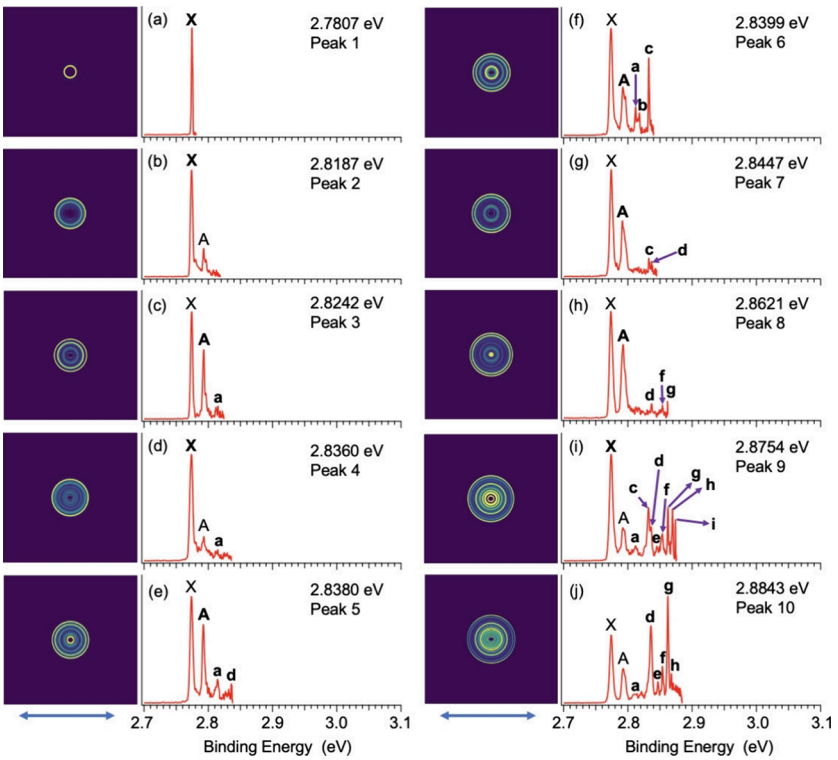

Figure 5. Resonant PE images and spectra of CN-Cp$^-$ at peaks 1−10 in the PDS (Figure 3 and Table 1). (a) 2.7807 eV (22,428 cm^{-1}), (b) 2.8187 eV (22,735 cm^{-1}), (c) 2.8242 eV (22,779 cm^{-1}), (d) 2.8360 eV (22,874 cm^{-1}), (e) 2.8380 eV (22,890 cm^{-1}), (f) 2.8399 eV (22,906 cm^{-1}), (g) 2.8447 eV (22,944 cm^{-1}), (h) 2.8621 eV (23,085 cm^{-1}), (i) 2.8754 eV (23,192 cm^{-1}), and (j) 2.8843 eV (23,264 cm^{-1}). The double arrow below the images represents the polarization direction of the laser.

The feature identified as S_0 on the higher BE region originates from electron signals detached from rovibrationally excited anions of the ground electronic state of CN-Cp$^-$, populated due to relaxation from the DBS following the absorption of the first photon. This signal is relatively weak in comparison to the direct R2PD peak, indicating a long-lived DBS for the CN-Cp$^-$ anion. Very weak signals are also discernible around 2.1 eV (inset, Figure 4) and they do not seem to be related to the ground state of CN-Cp$^-$. It will be shown below that these very weak signals come from another isomer of CN-Cp$^-$.

3.4. Resonant Photoelectron Imaging via Vibrational Feshbach Resonances. By tuning the detachment laser to the positions of the Feshbach resonances observed in Figure 3, we acquired 15 resonant PE spectra, as shown in Figure 5 for peaks 1−10 and in Figure S1 for peaks 11−15. Since first conducted for the phenoxide anion,[18] rPES via DBS of cryogenically cooled anions has proven to be valuable in obtaining detailed spectroscopic information about radical species.[14] In comparison to the nonresonant PE spectra depicted in Figure 2, the resonant PE spectra are much better resolved and exhibit enhancements in one or more vibronic features (highlighted in boldface in Figure 5 and Figure S1). Most notably, many new vibronic peaks (labeled from a to y) are observed, whereas no vibronic features can be resolved in the nonresonant PE spectra in Figures 1 and 2. The binding energies of all the observed vibronic peaks and their shifts relative to the 0−0 transition are summarized in Table 2.

4. DISCUSSION

4.1. Nonresonant Photoelectron Spectra of CN-Cp$^-$. The HOMO (b_1) and HOMO-1 (a_2) of CN-Cp$^-$ are both π orbitals, as shown in Figure 6. These two orbitals are nearly degenerate and are separated only by 0.089 eV at the B3LYP level. Thus, the ground state PES band (X) should be from detachment from the HOMO (b_1), whereas the peak A should be the origin of the excited state due to detachment from the HOMO-1 (a_2). The angular distributions and near-threshold behavior of the X and A peaks are consistent with the symmetries of the HOMO (b_1) and HOMO-1 (a_2). According to the PE images in Figure 2c,d, the two peaks exhibit ($s + d$)-wave angular distributions with their maximum intensity perpendicular to the laser polarization (see Table S1 for the β parameters). The spectrum for peak X in Figure 2a is almost isotropic ($\beta = 0.03$, Table S1), suggesting the s-partial wave is dominant near threshold. This observation is consistent with the onset in the photodetachment spectrum in Figure 3, which indicates an s-wave behavior near the detachment threshold. On the other hand, the d-partial wave dominates near threshold for peak A as a result of detachment from the a_2 HOMO-1, resulting in the negative β values (Table S1) and the decreased relative intensity of peak A as the photon energy is decreased (Figure 2) according to the Wigner threshold law.[36] The current observations for the different threshold behaviors for peaks X and A are consistent with our previous study on the threshold photodetachment behaviors of the pyrrolide and imidazolide anions.[37] The HOMO of pyrrolide is an a_2 orbital, which gives rise to a d-wave detachment behavior near threshold, whereas the HOMO of imidazolide is a b_1 orbital, which gives rise to an s-wave detachment behavior near threshold.

The parent $C_5H_5^-$ anion with D_{5h} symmetry has a degenerate π HOMO (e_1''), resulting in a degenerate ground state ($^2E_1''$) for the C_5H_5 radical (Figure 7), which is subject to

https://doi.org/10.1021/acs.jpca.4c07624
J. Phys. Chem. A 2025, 129, 1060−1067

Table 2. Observed Vibronic Peaks in the Resonant Photoelectron Spectra (Figure 5 and Figure S1)

peak	BE (eV)[a]	BE (cm^{-1})[a]	shift (cm^{-1})[b]
X	2.7741(3)	22,375(2)	0
A	2.7929 (7)	22,526 (6)	151
a	2.8121(10)	22,681 (8)	306
b	2.8180(13)	22,729 (10)	354
c	2.8325(3)	22,846 (2)	471
d	2.8358(9)	22,872(7)	497
e	2.8468(9)	22,961(7)	586
f	2.8538(5)	23,018(4)	643
g	2.8622(18)	23,085(15)	710
h	2.8694(9)	23,143(7)	768
i	2.8739(8)	23,180(6)	805
j	2.8796(14)	23,226(11)	851
k	2.8883(8)	23,296(6)	921
l	2.8914(5)	23,321(4)	946
m	2.8988(5)	23,381(4)	1006
n	2.9010(6)	23,398(5)	1023
o	2.9058(12)	23,437(10)	1062
p	2.9086(16)	23,460(13)	1085
q	2.9131(1)	23,496(1)	1121
r	2.9172(21)	23,529(17)	1154
s	2.9257(32)	23,598(26)	1223
t	2.9325(3)	23,652(2)	1277
u	2.9385(3)	23,701(2)	1326
v	2.9419(2)	23,728(2)	1353
w	2.9515(13)	23,806(10)	1431
x	2.9604(18)	23,877(15)	1502
y	2.9743(2)	23,990(2)	1615

[a]The numbers in the parentheses denote the uncertainty associated with the last digit. For peaks b, i, r, and s, the uncertainty was evaluated by taking the full width at half-maximum. For all other peaks, the standard deviation was taken from all PE spectra. [b]The shift is relative to peak X.

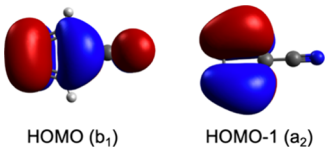

Figure 6. HOMO and HOMO-1 of the CN-Cp^- anion (isovalue = 0.02).

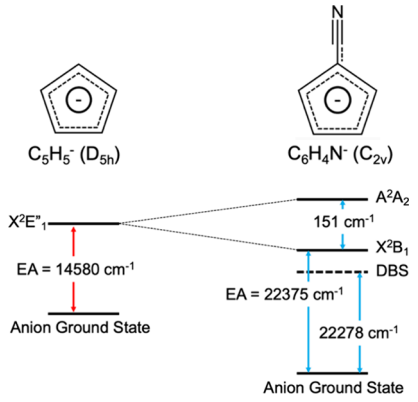

Figure 7. Schematic energy level diagrams of $C_5H_5^-$ vs CN-Cp^-. The EA for $C_5H_5^-$ is from ref 37.

Jahn–Teller distortion and the vibronic coupling has been studied extensively.[38−40] The lifting of this degeneracy has been observed in the deuterated cyclopentadienyl radical (C_5H_4D), where a splitting of 9 cm^{-1} is observed.[41] The low-lying excited state (A) observed for CN-Cp should be due to the splitting of the degenerate state in the parent C_5H_5 radical, as schematically shown in Figure 7. It is reasonable that the bulkier and more electron-withdrawing CN group in CN-Cp induces a splitting (151 cm^{-1}) much larger than that in C_5H_4D.

The CN-Cp^- anion has C_{2v} symmetry, where Franck–Condon allowed vibrational transitions typically involve A_1 modes, which are in-plane symmetric stretching or bending modes. The FC factors for the ground state transition are computed at the B3LYP/aug-cc-pVTZ level of theory and overlaid on top of the 3.0616 eV spectrum in Figure 8. Clearly,

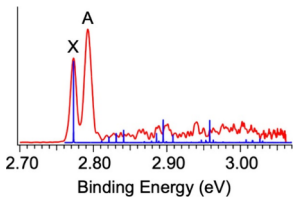

Figure 8. Comparison of the calculated FC factors (vertical lines) for the ground state detachment transition of CN-Cp^- with the nonresonant PE spectrum at 3.0616 eV.

the FC factors are not in good agreement with the experimental data. Much more complicated and congested vibronic transitions are observed experimentally; the PE spectra are not well resolved even for near threshold transitions (Figure 2). These complicated spectral features are likely a result of overlaps between the vibronic levels of the X and A states and possible vibronic couplings between them.

4.2. Comparison between the PD Spectrum and Nonresonant PE Spectrum. The photodetachment spectrum in Figure 3 reveals a number of distinct vibronic levels regarding the DBS. The peak below the threshold (labeled 0) indicates the zero-point level of the DBS, where the binding energy was measured to be 94 ± 5 cm^{-1}. Fifteen Feshbach resonances (1−15) arise from single-photon excitations to vibrational levels of the DBS, followed by vibrationally induced autodetachment. The distinct threshold and the above-threshold continuum reflect the cross sections of single-photon nonresonant detachment processes.

Since the diffuse dipole-bound electron has little effect on the structure of the neutral core, PD spectra often resemble the PE spectra, as we have observed in all the PDS of nonvalence states.[14,18−24] The high resolution PDS even allowed us to assign the vibronic features of the PES of the triazolide, which was not assignable on the basis of FC simulations.[42] The nonresonant PE spectrum of CN-Cp^- taken at 3.0616 eV (Figure 2d), red-shifted by 94 cm^{-1}, is superimposed on the PD spectrum in Figure S2 by aligning the 0−0 transition in the PE spectrum to peak 0 of the PD spectrum. There is no resemblance between the PDS and the nonresonant PES, because no vibronic features were resolved in the latter. We have not observed such instances before for any anion that contains a nonvalence excited state. This provides strong evidence for the vibronic coupling between the X and A states in CN-Cp. Apparently, specific vibronic levels in the DBS are enhanced due to stronger coupling between certain vibronic

https://doi.org/10.1021/acs.jpca.4c07624
J. Phys. Chem. A 2025, 129, 1060−1067

levels and the dipole-bound electrons. Such mode specific vibronic coupling in the DBS was observed in the phenoxide anion initially.[18,43]

4.3. R2PD PE Spectrum. The R2PD PEI via the zero-point level directly probes the nature of the DBS.[44−46] The first R2PD PEI via a DBS was conducted for the phenoxide anion,[18] revealing a distinct *p*-wave R2PD signal consistent with the σ-type dipole-bound orbital. We have also observed π-type DBSs revealed by the $(s + d)$ angular distributions in the R2PD PE images.[44,45] As illustrated in Figure 4, the R2PD PE image in the low binding energy region for CN-Cp$^-$ exhibits a clear *p*-wave angular distribution with a β value of 1.67, which is in agreement with the nature of a σ-type dipole-bound orbital for CN-Cp$^-$. Since the weakly dipole-bound electron does not affect the corresponding neutral core, the geometries and potential energy curves of the dipole-bound anion and the neutral are similar. Thus, photodetachment from the DBS to the neutral by the second photon is strictly adiabatic, that is, there is no Franck−Condon activity except the 0−0 transition. The adiabatic nature of electron detachment from the DBS has been demonstrated for bound-vibrational levels in several anions,[47,48] as well as from PE spectra of ground state dipole-bound anions.[8,49] The additional feature "S_0" at the high BE region in Figure 4 is assigned to detachment from rovibrationally excited states in the ground electronic state of CN-Cp$^-$. The rovibrationally excited states are produced by relaxation from the zero-point level of the DBS following the absorption of the first photon and are then detached by a second photon within the same laser pulse (∼5 ns duration), as observed in the phenoxide anion[14] and many other DBS-supporting anionic systems.[44−46,50] The spectrum in Figure 4 shows a prominent DBS peak, indicating a relatively long lifetime for the bound DBS level.

The weak nonzero signal starting at 2.13 eV leading up to S_0 is noteworthy. It turns out to be from a very weakly populated isomer of the CN-Cp$^-$ anion due to deprotonation from a different carbon atom on the 5-membered ring. A similar isomer was observed previously for the pyrrolide anion produced during electrospray.[37] In the current case, the isomer is due to deprotonation from the β-carbon, as shown in Figure S3. The computed ADE for this isomer at the B3LYP/aug-cc-pVTZ level of theory is 2.11 eV, consistent with the observed feature (Figure S3).

4.4. Resonant PE Images and Spectra. Resonant PE images and spectra were acquired by fixing the detachment laser wavelength to the 15 Feshbach resonances of the DBS, as displayed in Figure 5 and Figure S1. At these resonant wavelengths, there are two processes: 1) the nonresonant direct detachment process and 2) the resonant excitation to the vibrational levels of the DBS followed by autodetachment. Because the geometry of the DBS and that of the corresponding neutral are similar, the vibrational autodetachment obeys the $\Delta v = -1$ propensity rule under the harmonic approximation.[51,52] When the DBS vibrational level $\nu_x'^n$ is excited, the autodetachment enhances the $(n-1)^{\text{th}}$ vibrational level in the neutral molecule (ν_x^{n-1}). Similarly, for autodetachment from a combination level $(\nu_x'^n\nu_x'^m...)$ of the DBS, the neutral final state can be either $\nu_x'^{n-1}\nu_x'^m...$ or $\nu_x'^n\nu_x'^{m-1}...$, resulting in multiple enhanced peaks in the resonant PE spectra. Consequently, resonant PE spectra are highly non-Franck−Condon and the enhanced PES peaks are useful in the assignment of Feshbach resonances in PDS by comparing with the nonresonant PES.

In line with the $\Delta v = -1$ autodetachment propensity rule, excitation to the fundamental vibrational levels of the DBS should enhance the 0−0 transition. This is clearly observed in the resonant photoelectron spectra at peak 1 of the PDS for CN-Cp$^-$ (Figure 5a). The increase in the 0−0 transition due to autodetachment is further indicated by the more isotropic angular distribution, which is in contrast with the $(s + d)$-wave pattern seen in direct detachment processes. However, the other resonant PE spectra are difficult to assign because the nonresonant PE spectra display no resolved vibrational features for comparison with the resonant PE spectra. All the observed peaks in the PDS are given in Table 1 and those in the resonant PE spectra are reported in Table 2. These rich spectroscopic data will be valuable to be compared with future vibronic calculations for the CN-Cp radical.

5. CONCLUSIONS

In conclusion, cryogenically cooled CN-Cp$^-$ anions are studied using high-resolution photoelectron imaging, photodetachment spectroscopy, and resonant photoelectron imaging. The EA of the CN-Cp radical is measured to be 2.7741 ± 0.0003 eV (22,375 ± 2 cm^{-1}). A low-lying excited electronic state is observed for CN-Cp at 151 cm^{-1} above the ground state. The overlap between the vibrational levels of the ground state and the first excited state and their vibronic coupling lead to very complicated and congested photoelectron spectra. A dipole-bound state is observed for the CN-Cp$^-$ anion 94 cm^{-1} below the detachment threshold, along with 15 vibrational resonances. Resonant photoelectron spectra give rise to 26 well-resolved vibrational features. Even though these vibronic features cannot be definitively assigned, the rich spectroscopic data should stimulate theoretical calculations to unravel the vibronic coupling in the CN-Cp radial.

■ ASSOCIATED CONTENT

Supporting Information

The Supporting Information is available free of charge at https://pubs.acs.org/doi/10.1021/acs.jpca.4c07624.

Additional resonant PE images and spectra for CN-Cp$^-$, comparison of the PES with PDS, the isomer of CN-Cp$^-$, and the β values (PDF)

■ AUTHOR INFORMATION

Corresponding Authors

Dao-Fu Yuan − *Hefei National Research Center for Physical Sciences at the Microscale, University of Science and Technology of China, Hefei 230026, China;* orcid.org/0000-0001-8461-6889; Email: ydfu@ustc.edu.cn

Lai-Sheng Wang − *Department of Chemistry, Brown University, Providence, Rhode Island 02912, United States;* orcid.org/0000-0003-1816-5738; Email: lai-sheng_wang@brown.edu

Authors

Jisoo Kang − *Department of Chemistry, Brown University, Providence, Rhode Island 02912, United States*

Edward I. Brewer − *Department of Chemistry, Brown University, Providence, Rhode Island 02912, United States*

Yue-Rou Zhang − *Department of Chemistry, Brown University, Providence, Rhode Island 02912, United States*

Complete contact information is available at: https://pubs.acs.org/10.1021/acs.jpca.4c07624

Notes

The authors declare no competing financial interest.

■ ACKNOWLEDGMENTS

We would like to thank Dr. Yafu Guan and Prof. David R. Yarkony for helpful discussions regarding vibronic coupling effects. This work was supported by the U.S. Department of Energy, Office of Basic Energy Sciences, Chemical Sciences, Geosciences, and Biosciences Division, under Grant No. DE-SC0018679.

■ REFERENCES

(1) Tielens, A. G. G. M. Interstellar Polycyclic Aromatic Hydrocarbon Molecules. *Annu. Rev. Astron. Astrophys.* **2008**, *46*, 289−337.
(2) Duley, W. W. Polycyclic Aromatic Hydrocarbons, Carbon Nanoparticles and the Diffuse Interstellar Bands. *Faraday Discuss.* **2006**, *133*, 415−425.
(3) Byrne, A. N.; Xue, C.; Cooke, I. R.; McCarthy, M. C.; McGuire, B. A. Astrochemical Modeling of Propargyl Radical Chemistry in TMC-1. *Astrophys. J.* **2023**, *957*, 88.
(4) Fortenberry, R. C. Interstellar Anions: The Role of Quantum Chemistry. *J. Phys. Chem. A* **2015**, *119*, 9941−9953.
(5) Compton, R. N.; Carman, H. S., Jr.; Desfrancois, C.; Abdoul-Carime, H.; Schermann, J. P.; Hendricks, J. H.; Lyapustina, S. A.; Bowen, K. H. On the Binding of Electrons to Nitromethane: Dipole and Valence Bound Anions. *J. Chem. Phys.* **1996**, *105*, 3472−3478.
(6) Sommerfeld, T. Coupling Between Dipole-Bound and Valence States: the Nitromethane Anion. *Phys. Chem. Chem. Phys.* **2002**, *4*, 2511−2516.
(7) Desfrançois, C.; Abdoul-Carime, H.; Schermann, J.-P. Ground-State Dipole-Bound Anions. *Int. J. Mod. Phys. B* **1996**, *10*, 1339−1395.
(8) Hammer, N. I.; Hinde, R. J.; Compton, R. N.; Diri, K.; Jordan, K. D.; Radisic, D.; Stokes, S. T.; Bowen, K. H. Dipole-Bound Anions of Highly Polar Molecules: Ethylene Carbonate and Vinylene Carbonate. *J. Chem. Phys.* **2004**, *120*, 685−690.
(9) Qian, C. H.; Zhu, G. Z.; Wang, L. S. Probing the Critical Dipole Moment to Support Excited Dipole-Bound States in Valence-Bound Anions. *J. Phys. Chem. Lett.* **2019**, *10*, 6472−6477.
(10) McGuire, B. A.; Burkhardt, A. M.; Kalenskii, S.; Shingledecker, C. N.; Remijan, A. J.; Herbst, E.; McCarthy, M. C. Detection of the Aromatic Molecule Benzonitrile (c-C_6H_5CN) in the Interstellar Medium. *Science* **2018**, *359*, 202−205.
(11) McGuire, B. A.; Loomis, R. A.; Burkhardt, A. M.; Lee, K. L. K.; Shingledecker, C. N.; Charnley, S. B.; Cooke, I. R.; Cordiner, M. A.; Herbst, E.; Kalenskii, S.; et al. Detection of Two Interstellar Polycyclic Aromatic Hydrocarbons via Spectral Matched Filtering. *Science* **2021**, *371*, 1265−1269.
(12) Sita, M. L.; Changala, P. B.; Xue, C.; Burkhardt, A. M.; Shingledecker, C. N.; Lee, K. L. K.; Loomis, R. A.; Momjian, E.; Siebert, M. A.; Gupta, D.; et al. Discovery of Interstellar 2-Cyanoindene (2-C_9H_7CN) in GOTHAM Observations of TMC-1. *Astrophys. J. Lett.* **2022**, *938*, L12.
(13) McCarthy, M. C.; Lee, K. L. K.; Loomis, R. A.; Burkhardt, A. M.; Shingledecker, C. N.; Charnley, S. B.; Cordiner, M. A.; Herbst, E.; Kalenskii, S.; Willis, E. R.; et al. Interstellar Detection of the Highly Polar Five-Membered Ring Cyanocyclopentadiene. *Nat. Astron.* **2021**, *5*, 176−180.
(14) Zhu, G. Z.; Wang, L. S. High-Resolution Photoelectron Imaging and Resonant Photoelectron Spectroscopy via Noncovalent-Bound Excited States of Cryogenically-Cooled Anions. *Chem. Sci.* **2019**, *10*, 9409−9423.
(15) Ford, R. G.; Seitzman, H. A. The Microwave Spectrum and Dipole Moment of 1-Cyano-1,3-Cyclopentadiene. *J. Mol. Spectrosc.* **1978**, *69*, 326−329.
(16) Ishida, T.; Abe, H.; Nakajima, A.; Kaya, K. Electronic Spectrum of Jet-Cooled Cyanocyclopentadienyl Radical. *Chem. Phys. Lett.* **1990**, *170*, 425−429.
(17) Cullin, D. W.; Soundararajan, N.; Platz, M. S.; Miller, T. A. Laser-Induced Fluorescence Spectrum of the Cyanocyclopentadienyl Radical: A Band System Long Attributed to Triplet Phenylnitrene. *J. Phys. Chem.* **1990**, *94*, 8890−8896.
(18) Liu, H. T.; Ning, C. G.; Huang, D. L.; Dau, P. D.; Wang, L. S. Observation of Mode-Specific Vibrational Autodetachment from Dipole-Bound States of Cold Anions. *Angew. Chem., Int. Ed.* **2013**, *52*, 8976−8979.
(19) Liu, H. T.; Ning, C. G.; Huang, D. L.; Wang, L. S. Vibrational Spectroscopy of the Dehydrogenated Uracil Radical via Autodetachment of Dipole-Bound Excited States of Cold Anions. *Angew. Chem., Int. Ed.* **2014**, *53*, 2464−2468.
(20) Huang, D. L.; Liu, H. T.; Ning, C. G.; Wang, L. S. Vibrational State-Selective Autodetachment Photoelectron Spectroscopy from Dipole-Bound States of Cold 2-Hydroxyphenoxide: *o*-$HO(C_6H_4)O^-$. *J. Chem. Phys.* **2015**, *142*, 124309.
(21) Zhu, G. Z.; Huang, D. H.; Wang, L. S. Conformation-Selective Resonant Photoelectron Imaging from Dipole-Bound States of Cold 3-Hydroxyphenoxide. *J. Chem. Phys.* **2017**, *147*, No. 013910.
(22) Qian, C. H.; Zhang, Y. R.; Yuan, D. F.; Wang, L. S. Photodetachment Spectroscopy and Resonant Photoelectron Imaging of Cryogenically Cooled 1-Pyrenolate. *J. Chem. Phys.* **2021**, *154*, No. 094308.
(23) Zhang, Y. R.; Yuan, D. F.; Wang, L. S. Probing Dipole-Bound States Using Photodetachment Spectroscopy and Resonant Photoelectron Imaging of Cryogenically-Cooled Anions. *J. Phys. Chem. Lett.* **2023**, *14*, 7368−7381.
(24) Yuan, D. F.; Zhang, Y. R.; Wang, L. S. Dipole-Bound State, Photodetachment Spectroscopy, and Resonant Photoelectron Imaging of Cryogenically-Cooled 2-Cyanopyrrolide. *J. Phys. Chem. A* **2022**, *126*, 6416−6428.
(25) Wang, L. S. Perspective: Electrospray Photoelectron Spectroscopy: From Multiply-Charged Anions to Ultracold Anions. *J. Chem. Phys.* **2015**, *143*, No. 040901.
(26) Wang, L. S.; Ding, C. F.; Wang, X. B.; Barlow, S. E. Photodetachment Photoelectron Spectroscopy of Multiply Charged Anions Using Electrospray Ionization. *Rev. Sci. Instrum.* **1999**, *70*, 1957−1966.
(27) Wang, X. B.; Wang, L. S. Development of a Low-Temperature Photoelectron Spectroscopy Instrument Using an Electrospray Ion Source and a Cryogenically Controlled Ion Trap. *Rev. Sci. Instrum.* **2008**, *79*, No. 073108.
(28) Leon, I.; Yang, Z.; Liu, H. T.; Wang, L.S. The Design and Construction of a High-Resolution Velocity-Map Imaging Apparatus for Photoelectron Spectroscopy Studies of Size-Selected Clusters. *Rev. Sci. Instrum.* **2014**, *85*, No. 083106.
(29) Garcia, G. A.; Nahon, L.; Powis, I. Two-Dimensional Charged Particle Image Inversion Using a Polar Basis Function Expansion. *Rev. Sci. Instrum.* **2004**, *75*, 4989−4996.
(30) Dribinski, V.; Ossadtchi, A.; Mandelshtam, V. A.; Reisler, H. Reconstruction of Abel-Transformable Images: The Gaussian Basis-Set Expansion Abel Transform Method. *Rev. Sci. Instrum.* **2002**, *73*, 2634−2642.
(31) Cooper, J.; Zare, R. N. Angular Distribution of Photoelectrons. *J. Chem. Phys.* **1968**, *48*, 942−943.
(32) Frisch, M. J.; Trucks, G. W.; Schlegel, H. B.; Scuseria, G. E.; Robb, M. A.; Cheeseman, J. R.; Scalmani, G.; Barone, V.; Petersson, G. A.; Nakatsuji, H.;et al.*Gaussian 09*, rev. D.01; Gaussian, Inc.: Wallingford, CT, 2016.
(33) Pugliesi, I.; Müller-Dethlefs, K. The Use of Multidimensional Franck−Condon Simulations to Assess Model Chemistries: A Case Study on Phenol. *J. Phys. Chem. A* **2006**, *110*, 4657−4667.
(34) Laurie, V. W. Microwave Spectrum and Dipole Moment of Cyclopentadiene. *J. Chem. Phys.* **1956**, *24*, 635−636.
(35) Damiani, D.; Ferretti, L.; Gallinella, E. Structure of Cyclopentadiene from Microwave Spectra of Several Deuterated Species. *Chem. Phys. Lett.* **1976**, *37*, 265−269.
(36) Wigner, E. P. On the Behavior of Cross Sections Near Thresholds. *Phys. Rev.* **1948**, *73*, 1002−1009.

https://doi.org/10.1021/acs.jpca.4c07624
J. Phys. Chem. A 2025, 129, 1060−1067

(37) Zhang, Y. R.; Yuan, D. F.; Wang, L. S. Probing the Electronic Structure and Spectroscopy of Pyrrolyl and Imidazolyl Radicals using High-Resolution Photoelectron Imaging of Cryogenically Cooled Anions. *Phys. Chem. Chem. Phys.* **2022**, *24*, 6505−6514.
(38) Ichino, T.; Wren, S. W.; Vogelhuber, K. M.; Gianola, A. J.; Lineberger, W. C.; Stanton, J. F. The Vibronic Level Structure of the Cyclopentadienyl Radical. *J. Chem. Phys.* **2008**, *129*, No. 084310.
(39) Applegate, B. E.; Miller, T. A.; Barckholtz, T. A. The Jahn-Teller and Related Effects in the Cyclopentadienyl Radical. I. The Ab Initio Calculations of Spectroscopically Observable Parameters. *J. Chem. Phys.* **2001**, *114*, 4855−4868.
(40) Applegate, B. E.; Bezant, A. J.; Miller, T. A. The Jahn-Teller and Related Effects in the Cyclopentadienyl Radical. II. Vibrational Analysis of the $A^2A_2'' - X^2E_1''$ Electronic Transition. *J. Chem. Phys.* **2001**, *114*, 4869−4882.
(41) Yu, L.; Cullin, D. W.; Williamson, J. M.; Miller, T. A. High Resolution Laser Spectroscopy of Asymmetrically Deuterated Cyclopentadienyl Radicals: A Study of Vibronic Degeneracy Resolution and Jahn−Teller Distortion. *J. Chem. Phys.* **1993**, *98*, 2682−2698.
(42) Zhang, Y. R.; Yuan, D. F.; Wang, L. S. Probing the Strong Nonadiabatic Interactions in the Triazolyl Radical Using Photodetachment Spectroscopy and Resonant Photoelectron Imaging of Cryogenically-Cooled Anions. *J. Am. Chem. Soc.* **2022**, *144*, 16620−16630.
(43) Kang, D. H.; An, S.; Kim, S. K. Real-Time Autodetachment Dynamics of Vibrational Feshbach Resonances in a Dipole-Bound State. *Phys. Rev. Lett.* **2020**, *125*, No. 093001.
(44) Yuan, D. F.; Liu, Y.; Qian, C. H.; Zhang, Y. R.; Rubenstein, B. M.; Wang, L. S. Observation of a π-Type Dipole-Bound State in Molecular Anions. *Phys. Rev. Lett.* **2020**, *125*, No. 073003.
(45) Yuan, D. F.; Zhang, Y. R.; Qian, C. H.; Liu, Y.; Wang, L. S. Probing the Dipole-Bound State in the 9-Phenanthrolate Anion by Photodetachment Spectroscopy, Resonant Two-Photon Photoelectron Imaging, and Resonant Photoelectron Spectroscopy. *J. Phys. Chem. A* **2021**, *125*, 2967−2976.
(46) Yuan, D. F.; Liu, Y.; Qian, C. H.; Kocheril, G. S.; Zhang, Y. R.; Rubenstein, B. M.; Wang, L. S. Polarization of Valence Orbitals by the Intramolecular Electric Field from a Diffuse Dipole-Bound Electron. *J. Phys. Chem. Lett.* **2020**, *11*, 7914−7919.
(47) Zhu, G. Z.; Cheung, L. F.; Liu, Y.; Qian, C. H.; Wang, L. S. Resonant Two-Photon Photoelectron Imaging and Intersystem Crossing from Excited Dipole-Bound States of Cold Anions. *J. Phys. Chem. Lett.* **2019**, *10*, 4339−4344.
(48) Yuan, D. F.; Zhang, Y. R.; Qian, C. H.; Wang, L. S. Resonant Two-Photon Photoelectron Imaging and Adiabatic Detachment Processes from Bound Vibrational Levels of Dipole-Bound States. *Phys. Chem. Chem. Phys.* **2022**, *24*, 1380−1389.
(49) Ciborowski, S. M.; Liu, G.; Graham, J. D.; Buytendyk, A. M.; Bowen, K. H. Dipole-Bound Anions: Formed by Rydberg Electron Transfer (RET) and Studied by Velocity Map Imaging-Anion Photoelectron Spectroscopy (VMI-aPES). *Eur. Phys. J. D* **2018**, *72*, 139.
(50) Zhang, Y. R.; Yuan, D. F.; Qian, C. H.; Wang, L. S. Observation of A Dipole-Bound Excited State in 4-Ethynylphenoxide and Comparison with the Quadrupole-Bound Excited State in the Isoelectronic 4-Cyanophenoxide. *J. Chem. Phys.* **2021**, *155*, 124305.
(51) Berry, R. S. Ionization of Molecules at Low Energies. *J. Chem. Phys.* **1966**, *45*, 1228−1245.
(52) Simons, J. Propensity Rules for Vibration-Induced Electron Detachment of Anions. *J. Am. Chem. Soc.* **1981**, *103*, 3971−3976.

https://doi.org/10.1021/acs.jpca.4c07624
J. Phys. Chem. A 2025, 129, 1060−1067